Title: Impact of ocean phytoplankton diversity on phosphate uptake

Authors: Michael W. Lomas[1], Juan A. Bonachela[2,$], Simon A. Levin[2], and Adam C. Martiny[3,4,*]

Affiliations:

[1]Bigelow Laboratory for Ocean Sciences, East Boothbay, ME 04543

[2]Department of Ecology and Evolutionary Biology, Princeton University, Princeton, NJ 08544

[3]Department of Earth System Science, [4]Department of Ecology and Evolutionary Biology, University of California, Irvine, CA 92697

*Corresponding author:

3208 Croul Hall

Irvine, CA 92697

Phone: 949-824-9713

E-mail: amartiny@uci.edu

[$]Current address:

Juan.Bonachela@strath.ac.uk, MASTS Marine Population Modelling Group, Department of Mathematics and Statistics, University of Strathclyde, 26 Richmond Street, Glasgow, G1 1XH, Scotland, United Kingdom

Short title: Phytoplankton diversity and ocean phosphate uptake

Classification: Biological Sciences: Environmental Sciences

Keywords: Phosphate kinetics, Cyanobacteria, adaptive dynamics, eco-evolutionary dynamics.

Abstract

We have a limited understanding of the consequences of variations in microbial biodiversity on ocean ecosystem functioning and global biogeochemical cycles. A core process is macronutrient uptake by microorganisms, as the uptake of nutrients controls ocean CO_2 fixation rates in many regions. Here, we ask if variations in ocean phytoplankton biodiversity lead to novel functional relationships between environmental variability and phosphate (P_i) uptake. We analyzed P_i uptake capabilities and cellular allocations among phytoplankton groups and the whole community throughout the extremely P_i-depleted Western North Atlantic Ocean. P_i uptake capabilities of individual populations were well described by a classic uptake function but displayed adaptive differences in uptake capabilities that depend on cell size and nutrient availability. Using an eco-evolutionary model as well as observations of *in situ* uptake across the region, we confirmed that differences among populations lead to previously uncharacterized relationships between ambient P_i concentrations and uptake. Supported by novel theory, this work provides a fundamentally new empirical basis for describing and understanding assimilation of limiting nutrients in the oceans. Thus, it demonstrates that microbial biodiversity, beyond cell size, is important for understanding the global cycling of nutrients.

Significance statement

Nutrient uptake is a central property of ocean biogeochemistry; but our understanding of this process is based on lab cultures or bulk environmental studies. Thus, mathematical descriptions of nutrient uptake, at the heart of most biogeochemical models (including ones used by the Intergovernmental Panel on Climate Change), must rely on this limited information. Hence we have little knowledge of how natural phytoplankton populations vary in their abilities to take up key nutrients. Using new analytical techniques, this study provides the first comprehensive *in situ* quantification of nutrient uptake capabilities among dominant phytoplankton groups. Supported by a model that considers plastic ecological responses in an evolutionary context, this work further provides a fundamentally new framework for the integration of microbial diversity to describe and understand the controls of ocean nutrient assimilation.

\body

Introduction

The composition of microbial communities varies among different ocean regions and along environmental gradients (e.g., 1, 2). This variation includes phylogenetic, genomic, and functional diversity among and between hetero- or autotrophic groups. Presently, we have a limited understanding of the consequences of these different levels of microbial biodiversity on specific processes and more broadly on global ocean biogeochemical cycles (3). An important process is macronutrient uptake by microorganisms, as the uptake of nitrate and/or inorganic phosphate (P_i) controls ocean CO_2 fixation rates in many regions (4). Indeed, mathematical descriptions of nutrient uptake are at the heart of most marine ecosystem models (5). The ability of microorganisms to assimilate nutrients as a function of concentration is commonly described by a hyperbolic uptake kinetics curve (6, 7). Analogous to the classical Michaelis-Menten curves for enzyme kinetics (8), the parameters quantifying this relationship are the maximum uptake rate (V_{max}), the half saturation concentration (K_s), and the ratio of the two parameters named the nutrient affinity (α). Despite the importance of accurate descriptions of nutrient uptake capabilities for the understanding of competition and ocean biogeochemistry (7), our knowledge of these properties is mostly limited to lab studies of cultured strains (9). However, culture-based kinetics estimates would suggest plankton are proliferating at <25% of the growth rates observed in the oligotrophic subtropical gyres. Thus, we need to quantify this key process in naturally competing populations (10–12) and explain the discrepancies. Furthermore, we have a limited quantitative knowledge of *in situ* uptake capabilities under conditions where the focal nutrient is extremely depleted. The latter is

important as marine microorganisms like *Prochlorococcus* often have unique genomic adaptions to maximize nutrient assimilation under such conditions (13, 14).

To address this lack of knowledge for a globally relevant ecosystem process, we here aimed at identifying the influence of different levels of microbial biodiversity on *in situ* P_i uptake in the Western Subtropical North Atlantic Ocean. Phosphate plays a central role in regulating the functioning of microbial communities in this region as the surface waters likely have the lowest P_i concentration observed anywhere in the ocean (15). We used a combination of shipboard cell-sorting and isotopically labeled P_i to quantify nutrient uptake capabilities for the whole field community and four phytoplankton groups of different sizes – *Prochlorococcus*, *Synechococcus*, small eukaryotes (<20 μm), and the nitrogen fixer *Trichodesmium*. We asked: (i) Do the *in situ* P_i uptake capabilities differ *among* abundant phytoplankton groups, (ii) what is the variation in uptake capabilities *within* each group between environments, and (iii) what is the integrative effect of marine microbial diversity and environmental variability on nutrient uptake across the region? The answers to these questions will provide both a theoretical and empirical basis for describing how microbial diversity affects a core ocean ecosystem process.

Results

We first examined the uptake capabilities for the whole community and four phytoplankton groups – *Prochlorococcus*, *Synechococcus*, small eukaryotes (<20 μm), and the nitrogen fixer *Trichodesmium* (Figure 1 and S1) across a range of environments (Figure S2). When we experimentally added increasing concentrations of P_i, the nutrient uptake response closely resembled a hyperbolic shape for all discrete populations as well

as the whole community (R^2> 0.9, Figure 1 and S1). We then estimated the parameters K_s, V_{max} and affinity (α) (Table S1) and found significant (1-way ANOVA, $p < 0.05$) differences in K_s among phytoplankton groups (Figure S3 and Table S1). *Prochlorococcus* had the lowest average K_s followed by *Synechococcus*, small eukaryotic phytoplankton, and *Trichodesmium,* respectively. In comparison, the whole microbial community was characterized by K_s values between those of *Prochlorococcus* and *Synechococcus*, the most abundant autotrophs. There was also significant variation in V_{max} among phytoplankton lineages (1-way ANOVA, $p < 0.05$), and the order was analogous to K_s.

We then examined if differences in uptake abilities were related to cell size and found a significant positive relationship for both K_s and V_{max} (Figure 2, $p_{spearman} < 0.05$), but not affinity. The latter would suggest that small cells do not have a distinct competitive advantage at very low substrate concentrations. However, we also measured the P_i cell quota (Q_p) for all groups (Table S1) and observed that affinity normalized to Q_p ranked *Prochlorococcus* > *Synechococcus* > eukaryotic phytoplankton > *Trichodesmium*. An identical pattern was observed for V_{max} normalized to Q_p. Thus, *Prochlorococcus* had the highest potential for uptake in relation to demand at low concentrations, despite having a low absolute V_{max}.

In addition to size-dependent variations *across* phytoplankton groups, we also observed differences in nutrient uptake capabilities *within* each group. For example, samples 2 and 10 at BATS during the highly stratified late summer/early fall period consistently had a higher V_{max} but not K_s for the whole community and three discrete phytoplankton lineages in comparison to samples from the less stratified springtime (#4

and 5) (Figure 1 and Table S1). Similarly, we observed a higher V_{max} for a surface (#5) vs. 80 m sample (#6) (Figure S4). We hypothesized that these differences were related to P_i availability. To investigate this result further, we compared uptake capabilities to ambient P_i concentration at the time of sampling and found V_{max}, and especially affinity, were negatively correlated to P_i (Figure 3, $p_{ANCOVA} < 0.05$). In further support, V_{max} was lower in *Prochlorococcus* field populations from samples with higher P_i from the North Pacific Ocean (10). Thus, populations growing in low P_i environments showed significantly enhanced uptake capabilities.

We finally asked whether the presence of the observed physiologically (and possibly genetically) diverse populations would influence the link between nutrient availability and *in situ* uptake (V_{Pi}) across environments. To address this, we built an eco-evolutionary model in which, according to our observations, each lineage was influenced by a size-dependent scaling of K_s and V_{max} (resulting from adaptation) as well as a regulation of the concentration of transport proteins (and associated V_{max}) in response to ambient nutrient availability (i.e., acclimation) (Figure S5). This theoretical model predicted a relationship between ambient P_i and V_{Pi} that was very different from a traditional Michaelis-Menten type curve. Moreover, in contrast to a classic hyperbolic model, the emergent uptake curves accurately replicated our measurements of V_{Pi} of four phytoplankton groups in samples collected across the whole Western North Atlantic region (Figure 4 and S2). However, our model required specific allometries for each phytoplankton group, which suggested that size alone could not describe differences in P_i uptake between the lineages. Overall, these biodiversity effects also manifested themselves on the whole community V_{Pi}, where a linear fit replicated our observations

better than a hyperbolic one (Figure S6). These results highlight how the interaction of size and lineage diversity with physiological plasticity of phytoplankton had a direct impact on *in situ* nutrient uptake patterns in this region.

Discussion

Theoretical studies and culture data have both suggested that differences in microbial biodiversity can have an impact on nutrient uptake capabilities (5, 9, 16). Our results support culture studies showing an allometric scaling of K_s and V_{max} (9) including the lowest values in the small *Prochlorococcus* and *Synechococcus*. A recent compilation of available marine culture data does not report data for organisms as small as *Prochlorococcus* and *Synechococcus* (9), but based on their size, the values for *Prochlorococcus* and *Synechococcus* cells fall well below the predicted allometric line. Indeed, the best possible match between our eco-evolutionary model output and observations could only be achieved by using lineage-specific allometries for the traits involved. As a result, uptake capabilities of a given lineage cannot solely be described by specific cell-size-dependent K_s and V_{max} values.

Biodiversity may also influence nutrient uptake by a taxonomic group via differences in genomic content (14, 17, 18) and associated physiological capabilities of the cells (19, 20). We see strong support for a variation in uptake capabilities within populations that is likely linked to acclimation through the regulation of nutrient transporters in response to changes in the nutrient environment. To illustrate this further, we examined the ratio of V_{max} to Q_p, which can be interpreted as a proxy for the maximum growth rate (if we assume no leakage). However, we find values up to 27 d^{-1} for *Prochlorococcus* and 7.7 d^{-1} for *Synechococcus*, which are much higher than

previously described maximum growth rates for these groups (21, 22). This suggests that at least *Prochlorococcus* and *Synechococcus* have highly induced active P_i transporters at very low substrate levels. A maintenance of high V_{max} under strongly nutrient-limited conditions has been observed in marine diatom cultures (20), but this is the first demonstration of such V_{max} response mechanism in natural phytoplankton populations from the open ocean.

Identifying the linkages between marine biodiversity, environmental variation, and nutrient uptake rates has significant biogeochemical implications. A *Prochlorococcus* K_s of 0.8 nM reported here is the lowest value detected for any group yet, and we generally see high uptake rates for the whole community at low P_i. Thus, our data suggest that abundant phytoplankton groups can readily satisfy their P requirements, whether directly from P_i or from lyzed dissolved organic phosphorus, at less than 10 nM and thus lower the threshold for when P_i becomes limiting for growth. Our nutrient kinetics values are consistent with past studies of *Trichodesmium* (11) as well as the whole community (23) but add important quantitative information for specific unicellular lineages. Another biogeochemical consequence of our work concerns the parameterization of nutrient uptake in ocean models and associated skills in predicting future ocean chemical conditions, competition for limiting nutrients, and estimates of primary production. Several ocean biochemical models use K_s for P_i above 0.5 μM (24, 25), which results in gross model over-predictions of dissolved P_i concentrations in many oligotrophic regions. As a corollary, this results in under-estimation of primary production, which is important given the interest in predicting future rates of biological productivity in ocean gyres. Furthermore, given the hypothesis that open ocean gyres will continue to expand into the

future due to increasing stratification (26), these data suggest that *a priori* assumptions about reductions in ocean productivity need to be reevaluated.

We find strong support for a hyperbolic link between P_i and uptake for individual populations but the summed outcomes for P_i uptake by specific microbial lineages across environment gradients in P_i have a unique functional form. These results likely apply to a large fraction (~30%) of the global ocean surface area where P_i is similarly low. Thus, static K_s and V_{max} parameters for individual populations do not adequately describe the uptake rates across the region. Therefore, we recommend including these quantitative responses (e.g., much lower K_s values, feedback from plastic or adaptive responses, etc.) in ocean models if the aim is to accurately identify ecosystem processes in oligotrophic regions. This may be particularly pertinent if the goal is to predict future ocean biogeochemistry where increased warming may lead to decreases in P_i concentration (26) but not necessarily in phytoplankton abundances (27).

Methods

Sample collection. The data presented in this study were collected on 7 cruises throughout the Western North Atlantic Ocean (cruise X0606, X0705, X0804, BVAL 39, BVAL 46, AE1206, and AE1319). All samples for P_i uptake rates and kinetics experiments were collected in acid-cleaned Niskin bottles attached to a CTD rosette and kept in subdued lighting until experiments were initiated (< 1 h). Samples for whole community ambient uptake rates were collected from ~4 depths in the upper 60 m, while samples for taxon-specific ambient uptake rates were collected from 5 m, 40 m, and the deep chlorophyll maximum (DCM; ranging from 80 to 120 m) (28). *Trichodesmium*

colonies were collected from the near surface (roughly within the top 20 m) by vertically hauling a handheld 100 μm net. Single colonies were transferred a second time into fresh 0.2 μm-filtered water to reduce contamination of closely associated organisms, and subsequently separated by morphotype (either 'puff' with radial trichomes or 'raft' with parallel trichomes); only data for 'rafts' are presented here.

^{33}Phosphate incubations. The approach for ambient whole community and population-specific uptake rate measurements were previously published (28). Briefly, duplicate aliquots of 10 ml seawater were amended with 0.15 μCi (~80 pmol L^{-1}) additions of $H_3{}^{33}PO_4$ (3000 Ci mol^{-1}; PerkinElmer, USA), and incubated for 30 - 60 min in subdued lighting (~100 μmol photons m^{-2} s^{-1}) at ~23°C. This temperature was within ~3°C of the coolest/warmest *in situ* temperature from which the samples were collected. The duration of each incubation varied depending on turnover time of the added isotope, such that efforts were made to keep uptake to <25% of the tracer added. Duplicate killed control incubations were conducted for each station. Killed controls were amended with paraformaldehyde (0.5% final concentration) for 30 min prior to the addition of isotopic tracer and incubation. Whole community incubations were terminated by filtration onto 0.2 μm polycarbonate filters that were subsequently placed in glass scintillation vials. Population-specific ambient uptake incubations were terminated by the addition of paraformaldehyde (0.5% final concentration), and stored at 4°C until sorting (<12 h) as described in the next section.

Whole community and population-specific kinetics experiments were conducted by adding 0.15 μCi (~80 pM) of $H_3{}^{33}PO_4$ to ~10 replicate 10 ml seawater samples that were further amended by increasing additions of 'cold' KH_2PO_4 up to 100 nM. Samples

were incubated as above, but the incubations were terminated by the addition of KH_2PO_4 to a final concentration of 100 μM (29). Whole community samples were filtered onto 0.2 μm polycarbonate filters, and rinsed with an oxalate wash (30). Surface bound phosphate in population-specific samples was accounted for by subtracting ^{33}P counts for sorted populations to which 100 μM phosphate had been added prior to addition of the isotopic tracer. It is assumed that addition of such a high level of phosphate would result in negligible uptake of radioactive phosphate and thus any signal was attributed to surface absorption; this correction was always <2-3%. Population-specific kinetics experiments for samples collected in the deep chlorophyll maximum were first gravity concentrated and resuspended in phosphate-free Sargasso Sea surface water prior to incubation as described. Population-specific samples were stored at 4^{o}C in the dark until sorting (<3 h) as described in the next section. Kinetics experiments for *Trichodesmium* spp. were conducted in the same manner as above for whole community samples but with picked and rinsed colonies and increasing additions of 'cold' KH_2PO_4 up to 1000 nM.

Flow cytometry analysis and cell sorting. Samples were sorted on an InFlux cell sorter (BD, Seattle, WA) at an average flow rate of ~40 μL min^{-1}. Samples were sorted for *Prochlorococcus*, *Synechococcus*, and an operationally defined eukaryotic algae size fraction (eukaryotes >2 μm). A 100 mW blue (488 nm) excitation laser was used. After exclusion of laser noise gated on pulse width and forward scatter, autotrophic cells were discriminated by chlorophyll fluorescence (>650 nm), PE (585/30 nm), and granularity (side scatter). Sheath fluid was made fresh daily from distilled deionized water (Millipore, Billerica, MA) and molecular grade NaCl (Mallinckrodt Baker, Phillipsburg, NJ), pre-filtered through a 0.2 μm capsule filter (Pall, East Hills, NY), and a STERIVEX

sterile 0.22 μm inline filter (Millipore, Billerica, MA). Mean coincident abort rates were < 1% and mean recovery from secondary sorts (n = 25) was 97.5 ± 1.1% (data not shown). Spigot™ (BD Seattle, WA) and FCS Express V3™ (DeNovo Software, Seattle, WA) were used for data acquisition and post acquisition analysis, respectively. Sorted cells from each sample were gently filtered onto 0.2 μm Nucleopore polycarbonate filters, rinsed with copious amounts of 0.2 μm filtered seawater, an oxalate wash(30), and placed in a 7 ml scintillation vial for liquid scintillation counting.

Data analysis. Parameters for the hyperbolic nutrient uptake curves from all samples were estimated in SigmaPlot (Systat Software, San Jose, CA, Version 10) and the ANCOVA analysis was done with R. All other statistical analyses were done in Matlab (Mathworks, Natick, MA).

Biodiversity uptake model with adaptation and acclimation. In order to develop a theoretical model capable of predicting phosphate uptake and kinetic parameters V_{max} and K_s observed in the field across diverse populations, we used standard expressions for growth (Droop) and uptake (Michaelis-Menten). To these expressions, we added the possibility for phytoplankton to regulate kinetic parameters in reaction to environmental changes. We explicitly did not include the option of shifting expression between high and low affinity transporters as at least *Prochlorococcus* and *Synechococcus* only contain one type of P_i transporter system (14, 18). We then considered this ecological description within an evolutionary framework, which allowed us to calculate the most competitive within-taxon strain for each environmental setup. For each taxon, the compilation of winning strains in different locations provided the data we then contrasted with our observations (See supplementary information for further details). We did not include

Trichodesmium in this comparison, as we did not measure ambient uptake rates for this lineage.

Acknowledgements

We thank Stacey Goldberg and Céline Mouginot for assistance with cell-sorting and field sampling and Steven Allison and Jennifer Martiny for many helpful comments. Financial support for this work was provided by the National Science Foundation Dimensions of Biodiversity and Biological Oceanography programs.

Author contributions

MWL and ACM designed the research, MWL made the analytical measurements, ACM conducted the data analysis, JAB, ACM, and SAL developed the eco-evolutionary model and ACM wrote the paper with input from all authors.

References

1. Rusch DB et al. (2007) The Sorcerer II Global Ocean Sampling Expedition: Northwest Atlantic through Eastern Tropical Pacific. *PLoS Biol* 5:e77.

2. Zinger L et al. (2011) Global Patterns of Bacterial Beta-Diversity in Seafloor and Seawater Ecosystems. *PLoS One* 6:e24570.

3. Arrigo KR (2005) Marine microorganisms and global nutrient cycles. *Nature* 437:349–355.

4. Moore JK, Doney SC, Kleypas JA, Glover DM, Fung IY (2002) An intermediate complexity marine ecosystem model for the global domain. *Deep-Sea Res Pt II* 49:403–462.

5. Franks PJS (2009) Planktonic ecosystem models: perplexing parameterizations and a failure to fail. *J Plankton Res* 31:1299–1306.

6. Dugdale RC (1967) Nutrient limitation in the sea: Dynamics, identification and significane. *Limnol Oceanogr* 12:685–695.

7. Titman D (1976) Ecological competition between algae: experimental confirmation of resource-based competition theory. *Science (80-)* 192:463–465.

8. Michaelis L, Menten ML (1913) The kenetics of the inversion effect. *Biochem Z* 49:333–369.

9. Edwards K, Thomas M, Klausmeier CA, Litchman E (2012) Allometric scaling and taxonomic variation in nutrient utilization traits and maximum growth rate of phytoplankton. *Limnol Oceanogr* 57:554–566.

10. Björkman KM, Duhamel S, Karl DM (2012) Microbial group specific uptake kinetics of inorganic phosphate and adenosine-5í-triphosphate (ATP) in the North Pacific Subtropical Gyre. *Front Microbiol* 3:189. DOI: 10.3389/fmicb.2012.00189.

11. Orchard ED, Ammerman JW, Lomas MW, Dyhrman ST (2010) Dissolved inorganic and organic phosphorus uptake in the Sargasso Sea: variability in *Trichodesmium* and the microbial community. *Limnol Oceanogr* 55:1390–1399.

12. Sohm JA, Capone DG (2006) Phosphorus dynamics of the tropical and subtropical North Atlantic: *Trichodesmium* spp. versus bulk plankton. *Mar Ecol Prog Ser* 317:21–28.

13. Martiny AC, Huang Y, Li WZ (2009) Occurrence of phosphate acquisition genes in *Prochlorococcus* cells from different ocean regions. *Environ Microbiol* 11:1340–1347.

14. Martiny AC, Coleman ML, Chisholm SW (2006) Phosphate acquisition genes in *Prochlorococcus* ecotypes: Evidence for genome-wide adaptation. *Proc Natl Acad Sci U S A* 103:12552–12557.

15. Mather RL et al. (2008) Phosphorus cycling in the North and South Atlantic Ocean subtropical gyres. *Nat Geosci* 1:439–443.

16. Chisholm SW (1992) in *Primary Productivity and Biogeochemical Cycles in the Sea*, eds Falkowski PG, Woodhead AD (Plenum Press, New York), pp 213–237.

17. Martiny AC, Kathuria S, Berube PM (2009) Widespread metabolic potential for nitrite and nitrate assimilation among *Prochlorococcus* ecotypes. *Proc Natl Acad Sci* 106:10787–10792.

18. Scanlan DJ et al. (2009) Ecological genomics of marine picocyanobacteria. *Microbiol Mol Biol Rev* 73:249–299.

19. Rhee G-Y (1973) A continuous culture study of phosphate uptake, growth rate and polyphosphate in *Scenedesmus sp. J Phycol* 9:495–506.

20. Goldman JC, Glibert PM (1983) in *Nitrogen in the marine environment*, eds Carpenter EJ, Capone DG (Academic Press, New York), pp 233–273.

21. Moore LR, Goericke R, Chisholm SW (1995) Comparative physiology of *Synechococcus* and *Prochlorococcus*: influence of light and temperature on growth, pigments, fluorescence and absorptive properties. *Mar Ecol Prog Ser* 116:259–275.

22. Shalapyonok A, Olson RJ, Shalapyonok LS (1998) Ultradian growth in *Prochlorococcus* spp. *Appl Environ Microbiol* 64:1066–1069.

23. Ammerman JW, Hood RR, Case DA, Cotner JB (2003) Phosphorus deficiency in the Atlantic: An emerging paradigm in oceanography. *Eos, Trans Am Geophys Union* 84:165. DOI: 10.1029/2003EO180001.

24. Kane A et al. (2011) Improving the parameters of a global ocean biogeochemical model via variational assimilation of in situ data at five time series stations. *J Geophys Res* 116. DOI: 10.1029/2009JC006005.

25. Parekh P, Follows MJ, Boyle EA (2005) Decoupling of iron and phosphate in the global ocean. *Global Biogeochem Cycles* 19. DOI: 10.1029/2004GB002280.

26. Polovina JJ, Howell EA, Abecassis M (2008) Ocean's least productive waters are expanding. *Geophys Res Lett* 35. DOI: 10.1029/2007GL031745.

27. Flombaum P et al. (2013) Present and future global distributions of the marine Cyanobacteria *Prochlorococcus* and *Synechococcus*. *Proc Natl Acad Sci U S A* 110:9824–9829.

28. Casey JR et al. (2009) Phytoplankton taxon-specific orthophosphate (Pi) and ATP utilization in the western subtropical North Atlantic. *Aquat Microb Ecol* 58:31–44.

29. Larsen A, Tanaka T, Zubkov M V, Thingstad TF (2008) P-affinity measurements of specific osmotroph populations using cell-sorting flow cytometry. *Limnol Oceanogr* 6:355–363.

30. Tovar-Sanchez A et al. (2003) A trace metal clean reagent to remove surface-bound iron from marine phytoplankton. *Mar Chem* 82:91–99.

31. Casey JR, Aucan JP, Goldberg SR, Lomas MW (2013) Changes in partitioning of carbon amongst photosynthetic pico- and nano-plankton groups in the Sargasso Sea in response to changes in the North Atlantic Oscillation. *Deep-Sea Res Pt II* 93:58–70. DOI: 10.1016/j.dsr2.2013.02.002.

Legends

Figure 1. *In situ* phosphate uptake curves for the whole community and most abundant phytoplankton groups. The lines represent the best fit of a hyperbolic curve. Each row represents the whole community or specific population and each column represents a discrete station as listed in Table S1 and noted at the top of the panels. In panels B, F, I, and M, data from both October and March are shown as denoted in the legend in panel F. Panels C, G, J, and N show samples from 39N taken approximately one year apart. Triangle symbols and associated error bars represent the mean +/- stdev of duplicate experiments at this station.

Figure 2. Relationship between K_s, V_{max}, and cell mass across phytoplankton groups. Due to difficulties of accurately estimating cell volume, we used cellular carbon biomass as a proxy for cell size (31).

Figure 3. Relationships between the ambient P_i concentration and uptake capabilities (i.e., K_s, V_{max}, and α) for the whole community and *Prochlorococcus*, *Synechococcus*, and eukaryotic phytoplankton populations.

Figure 4. Relationship between *in situ* phosphate uptake rates (V_{pi}, black dots) and the ambient P_i concentration. The dashed lines are predictions from our eco-evolutionary model and the solid lines are traditional Michaelis-Menten functions applied to each

405 phytoplankton group. The Michaelis-Menten curves are based on the mean values for K_s and V_{max} (Table S1).

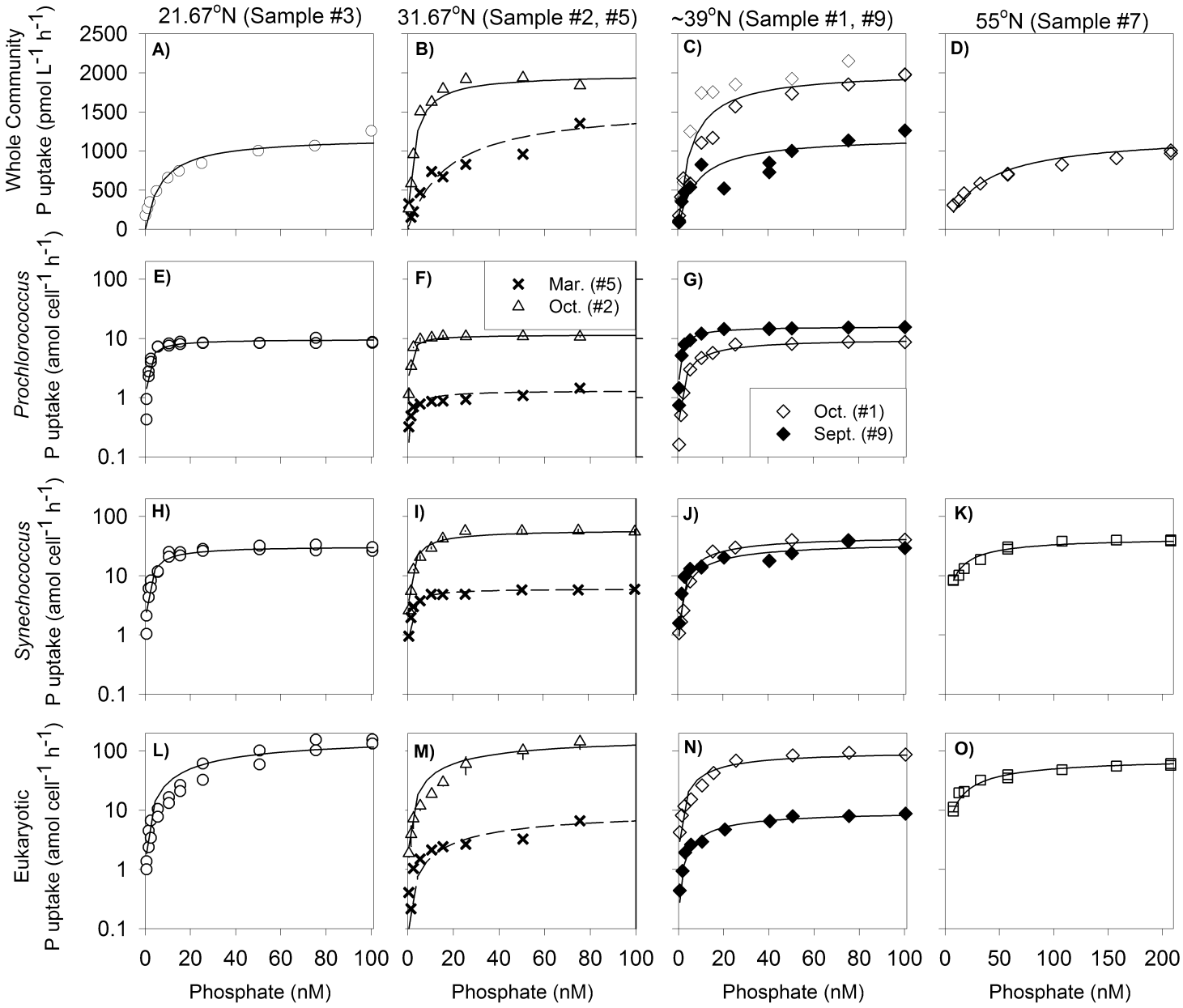
21.67°N (Sample #3)
31.67°N (Sample #2, #5)
~39°N (Sample #1, #9)
55°N (Sample #7)
Whole Community
P uptake (pmol L-1 h-1)
Prochlorococcus
P uptake (amol cell-1 h-1)
Synechococcus
P uptake (amol cell-1 h-1)
Eukaryotic
P uptake (amol cell-1 h-1)
A)
B)
C)
D)
E)
F)
G)
H)
I)
J)
K)
L)
M)
N)
O)
Mar. (#5)
Oct. (#2)
Oct. (#1)
Sept. (#9)
Phosphate (nM)
Phosphate (nM)
Phosphate (nM)
Phosphate (nM)

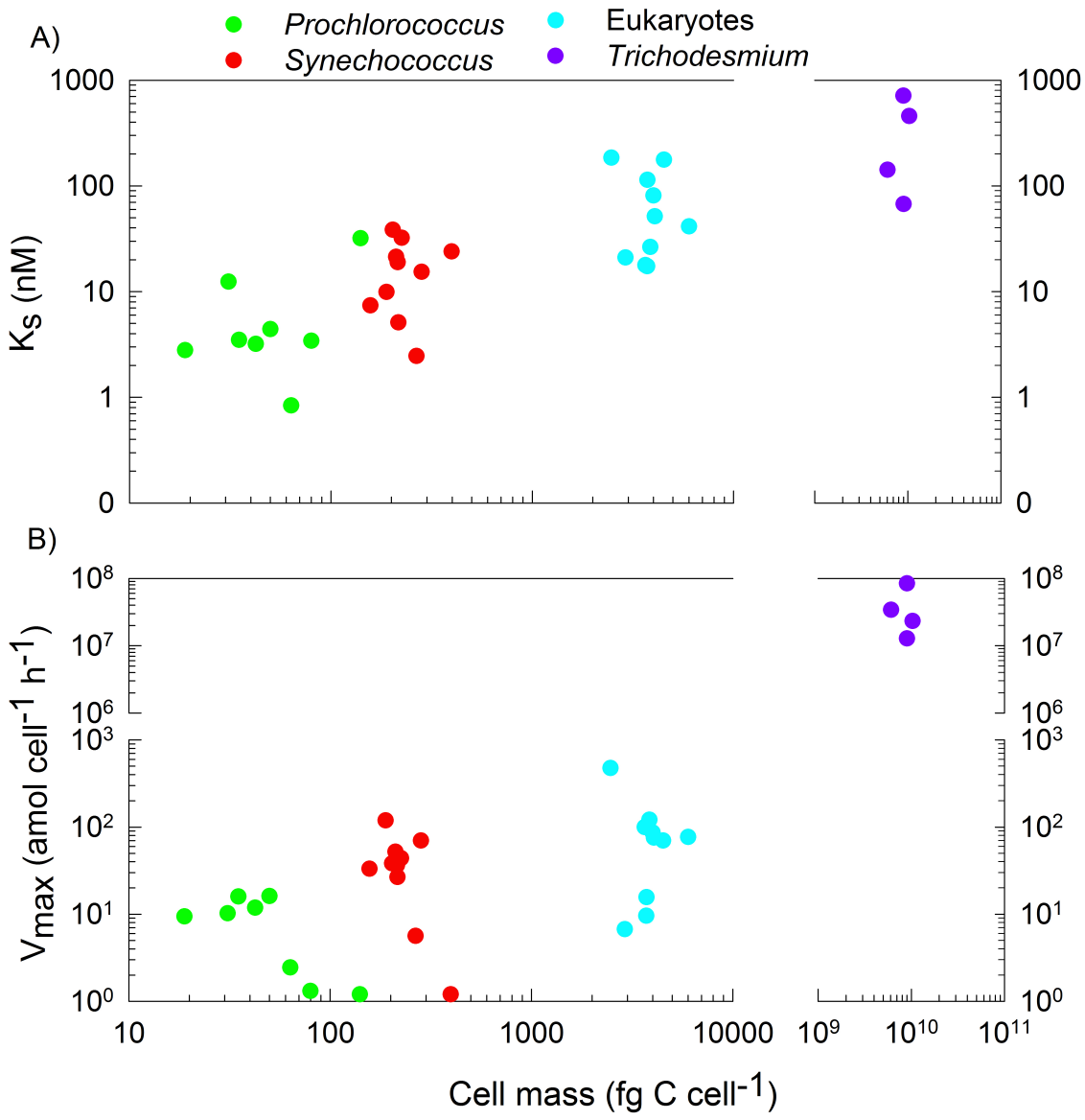
A)
Prochlorococcus
Synechococcus
Eukaryotes
Trichodesmium
Ks (nM)
1000
100
10
1
0
B)
Vmax (amol cell-1 h-1)
10^8
10^7
10^6
10^3
10^2
10^1
10^0
10
100
1000
10000
10^9
10^10
10^11
Cell mass (fg C cell-1)

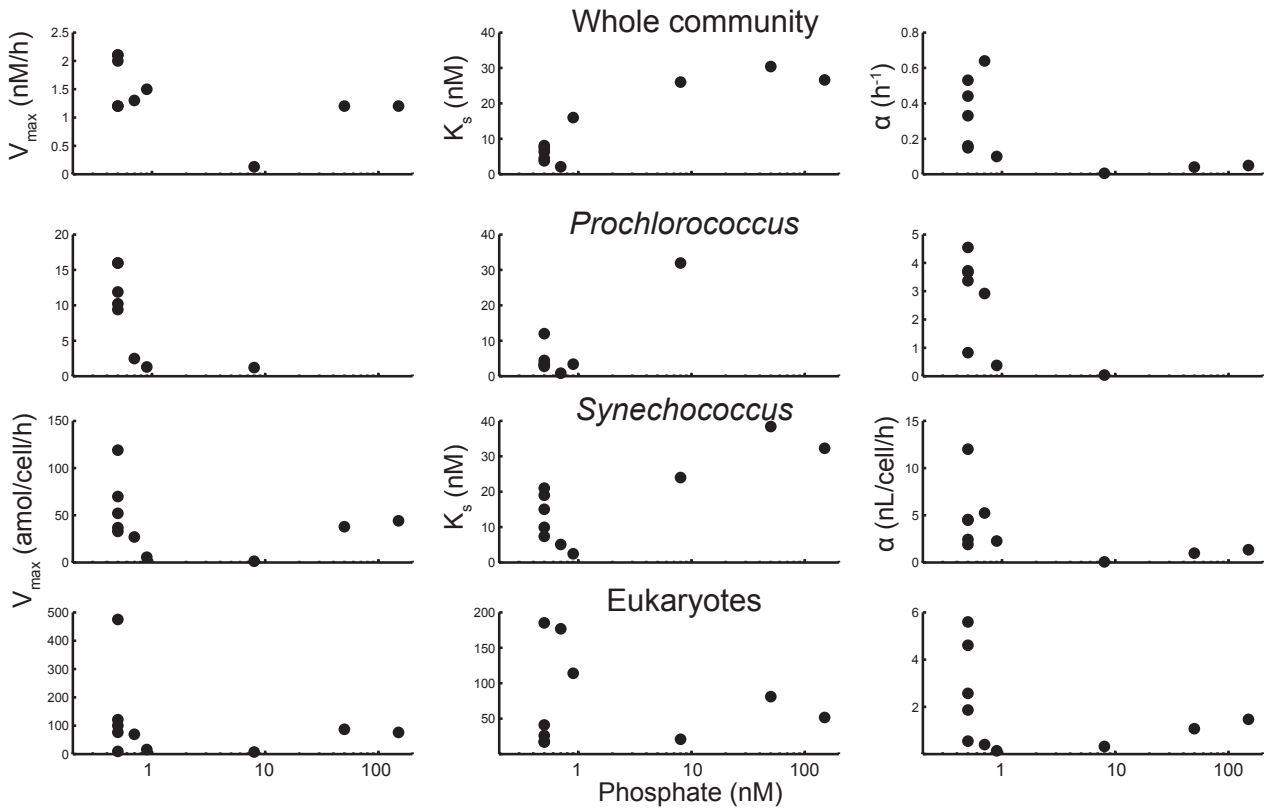
Whole community
Prochlorococcus
Synechococcus
Eukaryotes
V_{max} (nM/h)
K_s (nM)
α (h^{-1})
V_{max} (amol/cell/h)
K_s (nM)
α (nL/cell/h)
Phosphate (nM)

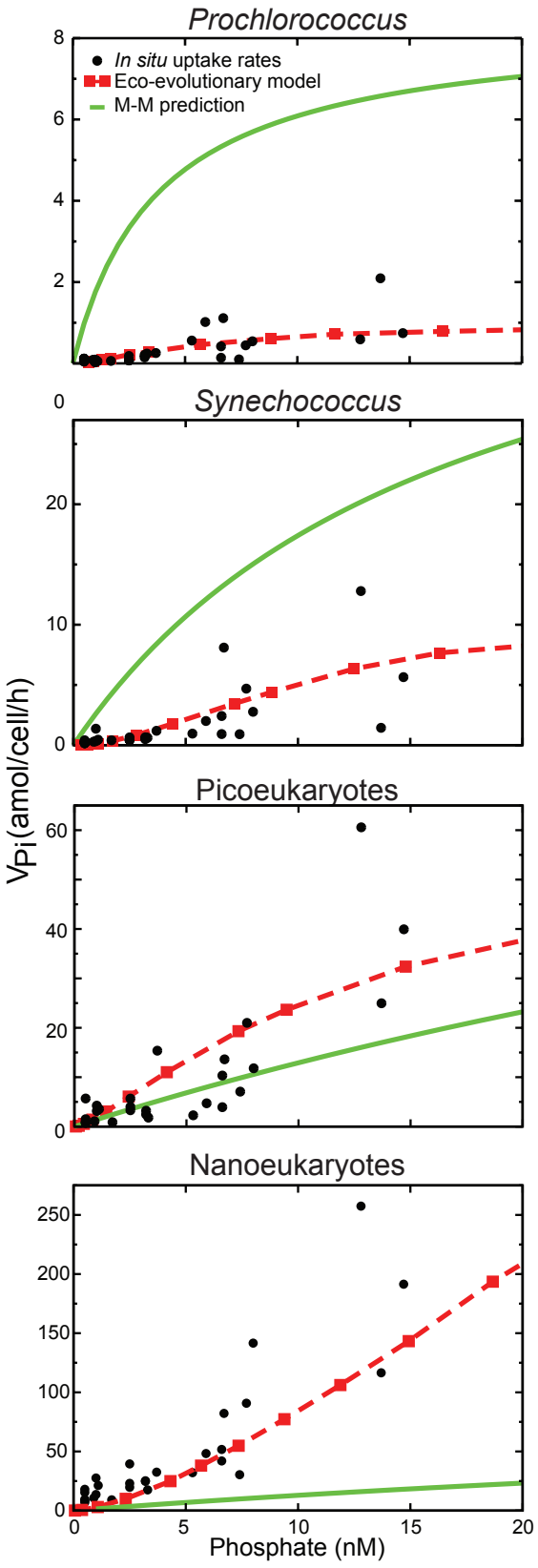
Prochlorococcus
In situ uptake rates
Eco-evolutionary model
M-M prediction
Synechococcus
Picoeukaryotes
Nanoeukaryotes
VPi(amol/cell/h)
Phosphate (nM)

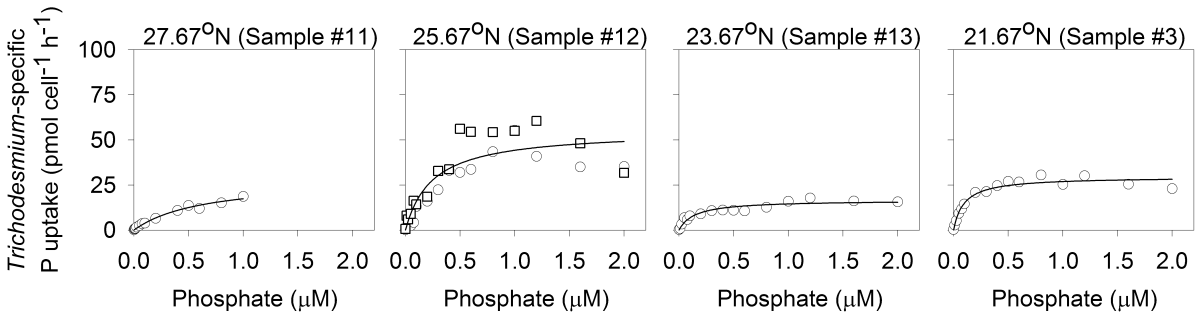
27.67°N (Sample #11)
25.67°N (Sample #12)
23.67°N (Sample #13)
21.67°N (Sample #3)
Trichodesmium-specific P uptake (pmol cell-1 h-1)
100
75
50
25
0
0.0 0.5 1.0 1.5 2.0
Phosphate (μM)

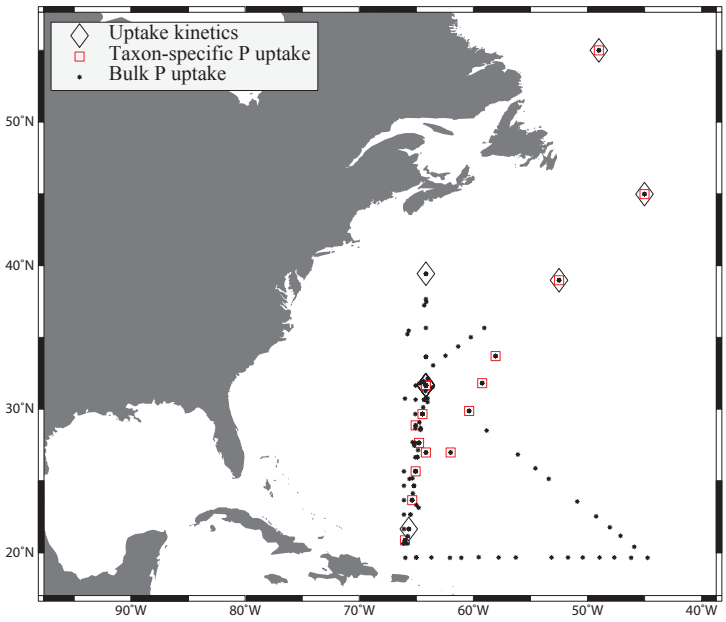
Uptake kinetics
Taxon-specific P uptake
Bulk P uptake
50°N
40°N
30°N
20°N
90°W
80°W
70°W
60°W
50°W
40°W

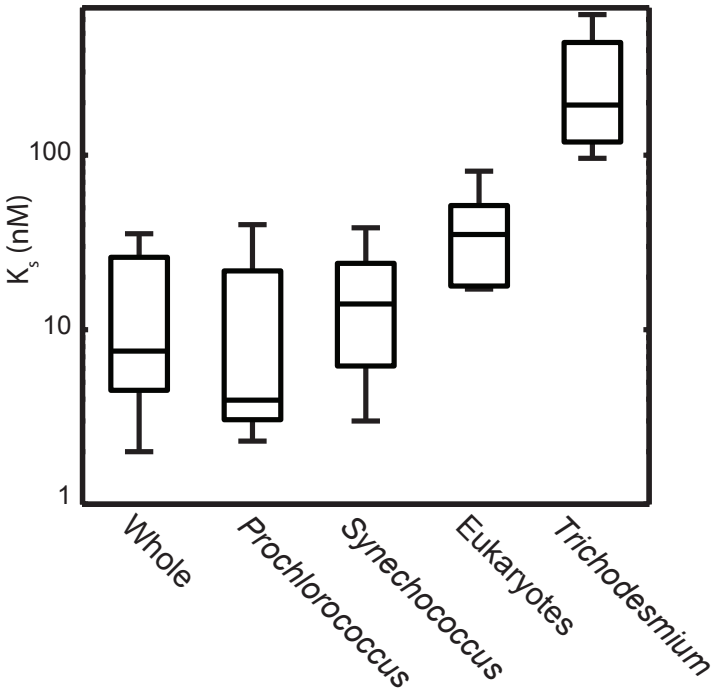
100
10
1
K_s (nM)
Whole
Prochlorococcus
Synechococcus
Eukaryotes
Trichodesmium

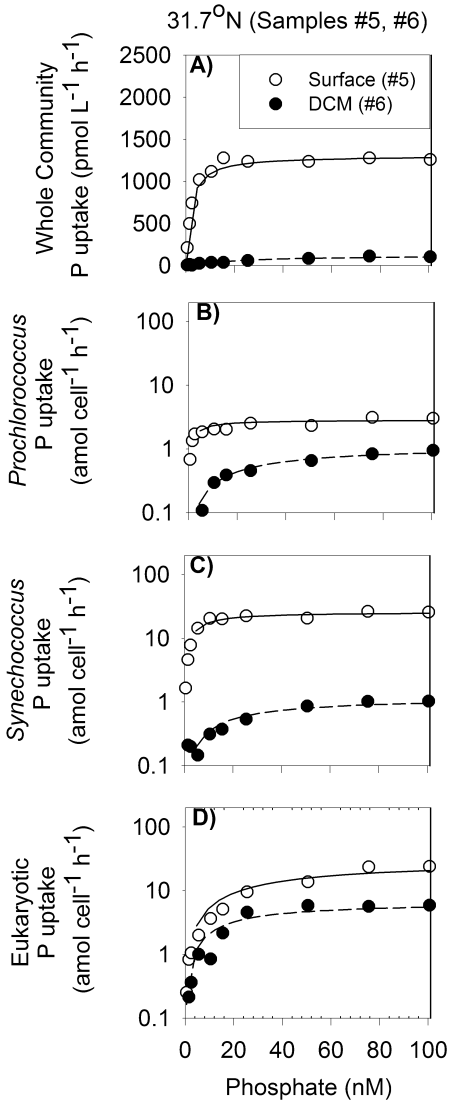
31.7°N (Samples #5, #6)
A)
Surface (#5)
DCM (#6)
Whole Community P uptake (pmol L-1 h-1)
2500
2000
1500
1000
500
0
B)
Prochlorococcus P uptake (amol cell-1 h-1)
C)
Synechococcus P uptake (amol cell-1 h-1)
D)
Eukaryotic P uptake (amol cell-1 h-1)
100
10
1
0.1
0
20
40
60
80
100
Phosphate (nM)

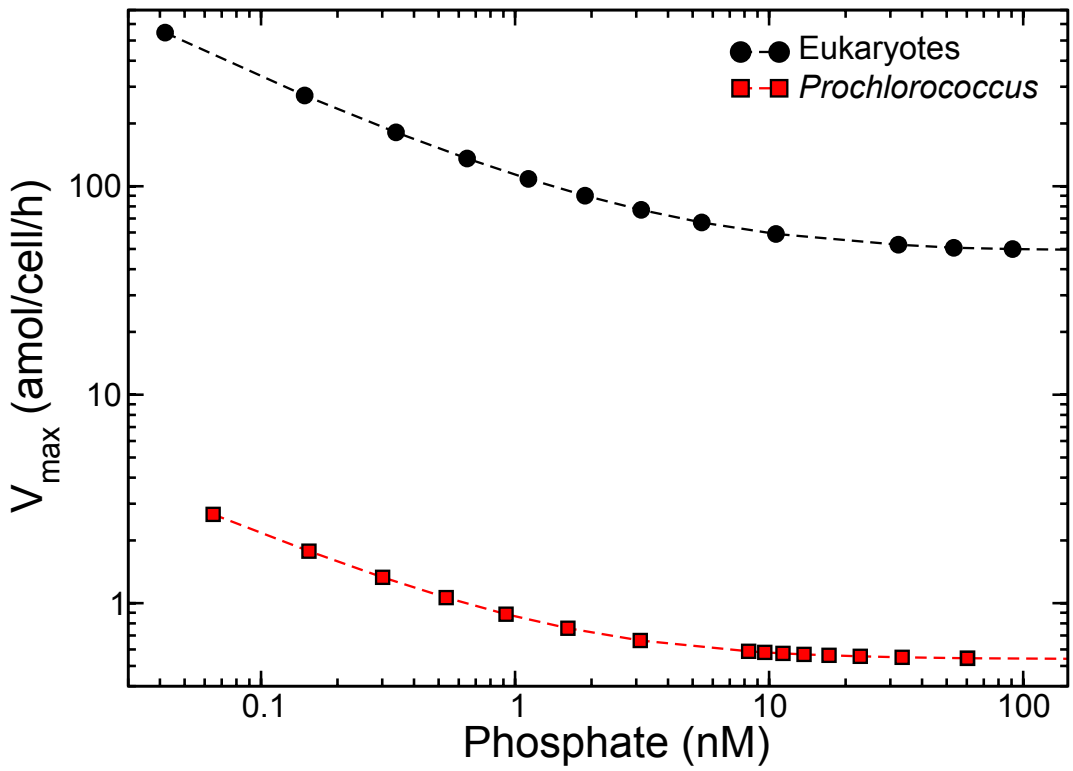
Eukaryotes
Prochlorococcus
100
10
1
V_{max} (amol/cell/h)
0.1
1
10
100
Phosphate (nM)

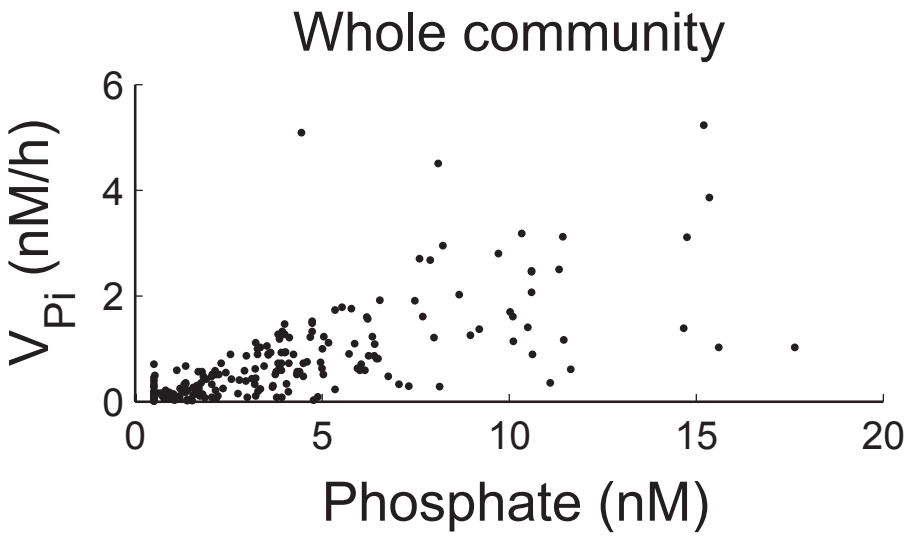
Whole community
V_{Pi} (nM/h)
6
4
2
0
0
5
10
15
20
Phosphate (nM)

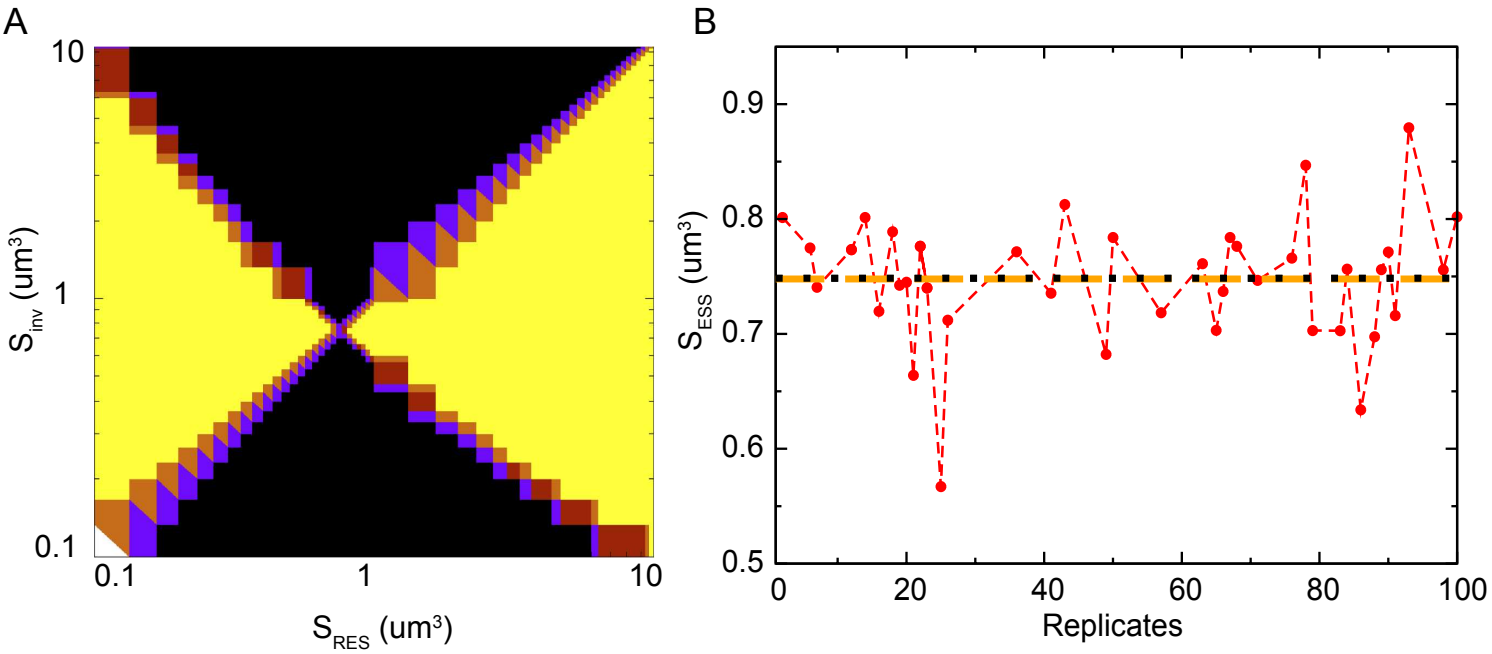
A
10
1
0.1
S_{inv} (um^3)
0.1
1
10
S_{RES} (um^3)
B
0.9
0.8
0.7
0.6
0.5
S_{ESS} (um^3)
0
20
40
60
80
100
Replicates

Supplementary Information:

P uptake Rate Calculations. Whole community and taxon-specific assimilation rates were calculated using the same equation as follows

410

$$V_{P_i} = \left[\frac{\beta_{sample}}{n}\right]^{\left(\frac{\Delta T \cdot \ln 2}{\lambda}\right)}\left[\frac{1}{\beta_{T_A}}\right]\left[\frac{P}{T_o}\right]$$

where V_{pi} is the cell-specific utilization rate (amol $^{33}P_i$ cell^{-1} hr^{-1}); β_{sample} and β_{TA} are the β-emission activities (counts min^{-1}) for the sorted sample and the total activity added, respectively; n is the number of cells sorted; ΔT is the elapsed time from ^{33}P isotopic 415 tracer addition to counting; T_o is the incubation duration; λ is the decay constant of ^{33}P (half life = 25.4 d); P is the ambient concentration of the P source (nmol L^{-1}). The method detection limit following this protocol is ~0.5 nM with a precision of $\pm$ 5% at 5 nM.

Phosphate cell quotas. Samples for taxon-specific cellular P quota (Q_p) were collected 420 as previously described with all samples except Sta. 2 representing newly available data (1). Briefly, whole water samples were collected and gently concentrated on a 0.4 μm polycarbonate filter. Cells were gently resuspended, and either sorted by flow cytometry immediately or fixed with paraformaldehyde (0.5% v/v final concentration) and stored at -80^{o}C until they could be sorted. Once sorted, samples were filtered on 13 mm silver 425 filters (*Prochlorococcus* and *Synechococcus*) or GF/F filters (eukaryotes) and analyzed as particulate phosphorus samples using the ash-hydrolysis method (2, 3). All samples were corrected for filter blanks. Paired comparison of unfixed and fixed cells from the same station/depth found that fixation had no effect on estimates of cellular P content (data not

shown). No efforts were made to separate particulate inorganic from organic phosphorus so data are simply referred to as particulate phosphorus. For analysis, sample filters were placed in acid-cleaned (10% HCl) and pre-combusted glass scintillation vials along with 2 ml of 17 mM $MgSO_4$, dried down at 80-90°C and then combusted at 500°C for 2 *h*. After cooling to room temperature, 5 ml of 0.2 M HCl was added to each vial and hydrolyzed at 80°C for 30 minutes. After cooling to room temperature, SRP mixed reagent was added (4), sample was clarified by centrifugation, and absorbance read at 885 nm. Samples were calculated against a potassium monobasic phosphate standard. Oxidation efficiency and standard recovery was tested with each sample run using an ATP standard solution and a certified phosphate standard (Ocean Scientific International Ltd. Phosphate Nutrient Standard Solution). In our laboratory, the precision of this method is ~9% at 2.5 nmol of P in the sample, and ~1% at 15 nmol of P in the sample. The method detection limit, defined herein as three times the standard deviation of the lowest standard (2.5 nM) is ~0.1 nmol L^{-1}.

Biodiversity uptake model with adaptation and acclimation

Model design: The Droop model links cell growth rates to the internal content of the most limiting nutrient (5). If Q represents the cell quota for such limiting nutrient (mol/cell), the growth rate μ (d^{-1}) follows the equation:

$$\mu(Q) = \mu_{max} \frac{\left(1 - Q_{min}/Q\right)}{\left(1 - Q_{min}/Q_{max}\right)}$$

where Q_{max} represents the maximum value for the quota (related to the maximum storage capacity of the cell), and Q_{min} is the minimum nutrient content required for growth. Note

that we chose a normalized version of the model (6), with which we ensured that the parameter μ_{max} expresses the (measurable) maximum value of the growth rate when Q reaches its maximum possible value. The cell quota, in turn, changes with time following a simple balance equation:

$$\frac{dQ}{dt} = V_{Pi} - \mu(Q)Q$$

where V_{Pi} represents uptake rate (in amol/cell/h). On the other hand, P_i uptake rate satisfies a Michaelis-Menten functional dependence:

$$V_{P_i} = \frac{V_{\max} P_i}{P_i + K_{eff}}$$

through which V_{Pi} depends on phosphate concentration, P_i, following a hyperbolic function modulated by the kinetic parameters, V_{max} and K_{eff}. The latter represents a diffusion-limitation correction that takes into account that the cell may develop a boundary layer due to the very low phosphate concentrations typical for the Western North Atlantic Ocean (7):

$$K_{eff} = K_S + \frac{V_{\max}}{4\pi D_{P_i} r_{cell}}$$

where r_{cell} is cell radius (in *dm*) and D_{Pi} (in dm^2/s) is the diffusivity constant for the focal resource (7). The dynamics of the population are represented by the simple equation:

$$\frac{dB}{dt} = \left(\mu(Q) - m\right)B$$

where B is the number of cells in the population, and m encodes any source of mortality for phytoplankton (in d^{-1}).

Next, we consider phytoplankton acclimation abilities by using an equation that links the change in time of the maximum uptake rate, V_{max}, to the nutritional state of the cell (i.e., its quota) (7). Through this equation, the dynamics of V_{max} (i.e. changes in the number of uptake proteins) depend on the internal content of the nutrient and, by extension, on the nutritional history of the cell. Thus, cells regulate the number of proteins in response to quota changes: when Q is low, the cell up-regulates the synthesis of such proteins to increase the absorbing area of the cell, thereby increasing the uptake rate; on the other hand, quotas close to the maximum storage limit allow the cell to down-regulate protein production and save associated synthesis and maintenance energy (7). All this phenomenology can be modeled, at the population level, using the equation (7, 8):

$$\frac{dV_{\max_B}(t)}{dt} = k_2\left[\nu H\left(1 - A_{rel}(t)\right)F\left(\frac{Q_{\max} - Q(t)}{Q_{\max} - Q_{\min}}\right)\right] - mV_{\max_B}(t)$$

where $V_{maxB} = B \cdot V_{max}$. H is a Heaviside function that introduces a limit to the maximum number of uptake proteins for the cell, set by the cell's surface area, with A_{rel} the ratio of absorbing to total cell area (which, therefore, depends on the number of proteins). k_2 is the assimilation rate (inverse of the handling or assimilation time):

$$k_2 = 4\pi D_{P_i} r_{site}$$

r_{site} is the absorbing radius of an uptake protein, and v is the maximum number of sites produced per unit time. $F(x) \in [-1, 1]$, is a sigmoid function, defined here as:

$$F\left(\frac{Q_{\max} - Q}{Q_{\max} - Q_{\min}}\right) = \frac{2}{1 + e^{-k_F\left(\frac{Q_{\max} - Q}{Q_{\max} - Q_{\min}}\right)}} - 1$$

k_F is a shape factor. The choice of F is justified because protein synthesis is the result of gene expression, typically represented by sigmoid functions (e.g., Hill function); however, other functional forms with similar Q-dependence do not alter the qualitative behavior of the ecological model (7).

Finally, we set chemostat conditions in which we altered the dilution rate, w (d^{-1}), in order to represent different locations. Thus, the dynamics for the resource concentration, R (in *nmol/l*) are given by:

$$\frac{dP_i}{dt} = w\left(P_{i0} - P_i\right) - V B$$

where P_{i0} is a (fixed) input of nutrient that can be tuned in chemostats.

Size-based parameterization. We considered size as the master trait representing phytoplankton strains. Thus, we chose a size-based parameterization; if s is cell size (or volume, in μm^3), we can express the allometric relationship for Q_{min}, Q_{max}, or v generically as $X=a_X \cdot s^{b_X}$ and used the across-taxon allometries proposed for phosphorus (9, 10). In addition, we devised an allometry for the parameter v that ensured that the qualitative behavior expected for V_{max} against P_i, relative to that of V_{Pi} [e.g. both should converge for high P_i (8, 11)], was observed regardless of cell size.

These allometries sufficed to find a qualitative agreement with our observations. In order to also reach a quantitative agreement, we needed to make use of the wide ranges provided in (9) for a_K, b_K, a_μ, and b_μ. This approach was justified by the fact that each taxon should be really represented by its own specific allometry for each trait. In this way, we assumed that eukaryotes shared an allometry for K_s (specifically, $a_K=2.00$ nM, $b_K=0.56$), different from that of Cyanobacteria ($a_K=3.98$ nM, $b_K=0.3$). Note that this

choice stretched the value of the coefficients a_K considerably beyond the limits obtained previously (9). Still, our selected coefficients and exponent ensured that smaller cells (Cyanobacteria) showed smaller K_s than bigger cells (eukaryotes). Similarly, we used b_μ=*-0.2* for eukaryotes and b_μ=*-0.3* for prokaryotes. Finally, we assumed that lineages were represented by different a_μ. Thus, we tuned the latter parameter to identify the emergent trait values for each lineage (Table S2).

Model evaluation. To replicate the observed P_i uptake kinetics curves (Figure 1), we focused on each taxon separately. Our assumption was that the biggest contribution to the measured taxon-specific curves arose from the dominant within-taxon strain in each location. Thus, we used the model described above to calculate the most competitive strain for a fixed value of a_μ, varying the dilution rate (that is, resource concentration) to replicate different locations. Further, we used three different methods to calculate the most competitive strain for each of those locations.

For the first method, we initialized our system by randomly assigning sizes ranging from 10^{-3} μm^3 to 10^8 μm^3 to 300-500 ecotypes, aiming at representing any possible within-taxon variability. Then, we let them compete for the single available resource. According to expectations, only one winner was observed per location. We used several replicates to obtain the characteristic winner of each location, due to the stochastic nature of the initial condition. The second method was devised to obtain the pairwise invasibility plot (PIP) for each location (Figure S7A). PIPs allow one to identify whether the strain is a local or a global winner in the trait space (12). Thus, we confronted a resident strain of size s with an immigrant strain of size s', and let them

compete until one single winner was observed. The process was then repeated sweeping all possible combinations of s and s' within specific ranges. Thus, we confirmed the results of the previous analyses, obtaining in all cases (global) winner's sizes in agreement with the previous simulations (Figure S7A). The third method considered evolution explicitly by using an eco-evolutionary framework (13). Starting from a random strain, new mutant strains are introduced according to the dynamics of the population and a fixed mutation rate. Competition for resources makes strains disappear; mutation and extinction allow the population to explore the trait space in a continuous way until the most competitive trait value is present. Due to its competitive advantage, this strain grows and resists invasion by any other strain. Thus, the average trait value for the population remains stable around the most competitive strain's trait value – i.e., the Evolutionarily Stable Strategy (ESS). Using this framework, the resulting ESS matched the sizes obtained with the other two methods above (Figure S7B). As an important additional result, the emergent V_{max} dependence on the size of the winning ecotypes shared, for all four lineages explored through simulations, a similar exponent $b_{Vmax}\sim 1$.

Finally, to replicate the variation in V_{max} observed under conditions of different phosphate availability (Figure 3), we used the same model and allometries described above but setting a fixed characteristic size representing each lineage. More specifically, we used s=0.1 μm^3 for *Prochlorococcus* and $s=20$ μm^3 for Eukaryotes. Then, we quantified the kinetic parameters V_{max}, K_s, and their ratio, α, resulting from the different stationary states (i.e. different nutrient conditions) obtained with chemostat environments varying the dilution rate, w (Figure S5).

Model with no regulation of transport proteins (i.e. only adaptation). In order to discern to what extent the combination of adaptation (evolutionary changes in cell size and, therefore, in size-related traits) and acclimation (regulation of transporters) was responsible for the observed patterns, we used a more simplistic approach in which we suppressed acclimation in the model above by keeping V_{max} constant. This approach was, thus, not able to replicate the kinetic curves.

Assuming that $dV_{max}/dt = 0$, we could use an allometry to initialize a constant V_{max}. We assumed a_{Vmax} =33.08 amol/cell/h, and $b_{Vmax} = 1$ (9). This simplification allowed us to obtain an explicit expression for the population growth rate and the ESS for size. By definition, the per-capita growth rate is given by:

$$\lambda = \frac{1}{B}\frac{dB}{dt} = \mu - m$$

By solving for stationary state, the quota dynamic equation, we obtain:

$$Q^* = \frac{V_{\max}\left(Q_{\max} - Q_{\min}\right)P_i^* + \mu_{\max}Q_{\min}Q_{\max}\left(P_i^* + K_S\right)}{\mu_{\max}Q_{\max}\left(P_i^* + K_S\right)}$$

And, replacing the expression above into the population growth rate:

$$\lambda = \frac{\mu_{\max}V_{\max}Q_{\max}}{V_{\max}\left(Q_{\max} - Q_{\min}\right) + \mu_{\max}Q_{\max}Q_{\min}} + \frac{P_i^*}{P_i^* + \left(\frac{\mu_{\max}Q_{\max}Q_{\min}K_S}{V_{\max}\left(Q_{\max} - Q_{\min}\right) + \mu_{\max}Q_{\max}Q_{\min}}\right)} - m$$

$$= \mu_{\max_M}\frac{P_i^*}{P_i^* + \kappa} - m$$

Thus, the population growth rate can be expressed as a Monod-like growth rate (14), with parameters given by:

$$\mu_{\max_M} = \frac{\mu_{\max}V_{\max}Q_{\max}}{V_{\max}\left(Q_{\max} - Q_{\min}\right) + \mu_{\max}Q_{\max}Q_{\min}}$$

$$\kappa = \frac{\mu_{\max} Q_{\max} Q_{\min} K_S}{V_{\max}\left(Q_{\max} - Q_{\min}\right) + \mu_{\max} Q_{\max} Q_{\min}}$$

The population growth rate can subsequently be used as invasion fitness. Therefore, the ESS is the point where the lines for $\lambda=0$ cross in a PIP (i.e. considering a resident and an invading phenotype, see above). The ESS is also a point where the resident's fitness reached a maximum (12) and fulfills:

$$\left.\frac{\partial \lambda}{\partial s}\right|_{P_i = P^*_{i\,res}} = 0$$

$$\left.\frac{\partial^2 \lambda}{\partial s^2}\right|_{P_i = P^*_{i\,res}} < 0$$

As a consequence, we can use the expression above to numerically estimate the size of the most competitive sizes within a taxon (i.e. fixed a_μ), for a variety of environments (i.e., for several w). Note that this simple model could not replicate quantitatively the observed patterns even although the allometry used for V_{max} is similar to that emerging from the complete model. Parameterizing this simpler model to replicate observations quantitatively involved fine-tuning most of the available allometric coefficients. In contrast, observed values emerged from the complete model by acknowledging essential functional differences between eukaryotes and Cyanobacteria (affecting here the allometry for K_s), and using a_μ as a taxon-specific parameter. In addition, the complete model allowed us to replicate the observed behavior for the kinetic parameters, also within realistic ranges. This discrepancy highlights the important role of acclimation in creating those patterns.

In summary, although this simple model and calculations showed that adaptation could be responsible for the qualitative shape of the uptake curves, only a combination of adaptation and acclimation was able to fully explain all the observed phenomenology.

600

Other model options. We also tried more phenomenological implementations of acclimation, such as replacing V_{max} by (15, 16):

$$V_{\max} = V_{\max}^{hi}\left(\frac{Q_{\max} - Q}{Q_{\max} - Q_{\min}}\right)$$

or a generalization of the above(8, 11):

605

$$V_{\max} = V_{\max}^{hi} - \left(\frac{Q - Q_{\min}}{Q_{\max} - Q_{\min}}\right)\left(V_{\max}^{hi} - V_{\max}^{lo}\right)$$

where the superscript *hi* and *lo* refer to the value of the maximum uptake rate for low and high P_i, respectively. The two expressions above showed an ultimate dependence of V_{max} on resource concentration qualitatively similar to that emerging from the mechanistic model used in the main text and observed in the data (i.e., V_{max} decreasing with P_i).

610 Unfortunately, although these expressions allowed for analytical solutions in the spirit of that presented in the previous section, none of them were able to replicate both qualitatively and quantitatively the behavior for uptake and kinetic parameters described in the main text. Thus, only a mechanistic implementation of such acclimation could reproduce the mentioned observations.

615

References

1. Martiny AC et al. (2013) Strong latitudinal patterns in the elemental ratios of marine plankton and organic matter. *Nat Geosci* 6:279–283.

2. Solorzano L, Sharp JH (1980) Determination of total dissolved phosphorus and particulate phosphorus in natural-waters. *Limnol Oceanogr* 25:754–757.

3. Lomas MW et al. (2010) Sargasso Sea phosphorus biogeochemistry: an important role for dissolved organic phosphorus (DOP). *Biogeosciences* 7:695–710.

4. Parsons TR, Maita Y, Lalli CM (1984) *A Manual of Chemical and Biological Methods for Seawater Analysis* (Pergamon Press).

5. Droop MR (1968) Vitamin B12 and Marine Ecology. IV. The Kinetics of Uptake, Growth and Inhibition in Monochrysis Lutheri. *J Mar Biol Assoc UK* 48:689–733.

6. Flynn KJ (2008) Use, abuse, misconceptions and insights from quota models - The Droop cell quota model 40 years on. *Oceanogr Mar Biol an Annu Rev Vol 46* 46:1–23.

7. Bonachela JA, Raghib M, Levin SA (2011) Dynamic model of flexible phytoplankton nutrient uptake. *Proc Natl Acad Sci U S A* 108:20633–20638.

8. Bonachela JA, Allison SD, Martiny AC, Levin SA (2013) A model for variable phytoplankton stoichiometry based on cell protein regulation. *Biogeosciences* 10:4341–4356.

9. Edwards K, Thomas M, Klausmeier CA, Litchman E (2012) Allometric scaling and taxonomic variation in nutrient utilization traits and maximum growth rate of phytoplankton. *Limnol Oceanogr* 57:554–566.

10. Grover JP (1989) Influence of cell shape and size on algal competitive ability. *J Phycol* 25:402–405.

11. Morel FMM (1987) Kinetics of nutrient uptake and growth in phytoplankton. *J Phycol* 23:137–150.

12. Dercole F, Rinaldi S (2008) *Introduction to Analysis of Evolutionary Processes: The Adaptive Dynamics Approach and Its Applications* (Princeton University Press).

13. Bonachela JA, Levin SA (2014) Evolutionary comparison between viral lysis rate and latent period. *J Theor Biol* 345:32–42.

14. Monod J (1950) La Technique De Culture Continue Theorie Et Applications. *Ann L Inst Pasteur* 79:390–410.

15. Geider RJ, MacIntyre HL, Kana TM (1998) A dynamic regulatory model of phytoplanktonic acclimation to light, nutrients, and temperature. *Limnol Oceanogr* 43:679–694.

16. Verdy A, Follows M, Flierl G (2009) Optimal phytoplankton cell size in an allometric model. *Mar Ecol Prog Ser* 379:1–12.

Figure legends

Figure S1. Phosphate uptake kinetics for the N_2-fixer *Trichodesmium* across the Western North Atlantic Ocean.

Figure S2. Map of samples used in this study, collected over multiple cruises led by Lomas in the western subtropical North Atlantic Ocean. This includes samples for P_i uptake kinetics, *in situ* uptake rates for the whole community as well as specific population, and other factors (particulate phosphate, dissolved inorganic phosphate, and P cell quota for specific populations). The taxon-specific P_i uptake data from two of the six cruises was previously published in Casey et al. 2009.

Figure S3. Phosphate uptake half-saturation concentrations (K_s) for the whole community and specific phytoplankton groups. The line in the box represents the median, the box the 25 and 75 percentile, and the whiskers cover approximately 99.3% of the data. K_s values are significantly different between groups (1-way ANOVA, $p < 0.05$).

Figure S4. Comparison of the P_i uptake kinetics for the whole community as well as specific phytoplankton populations between surface and DCM.

Figure S5. Eco-evolutionary model prediction for V_{max}. The predictions are for *Prochlorococcus* and eukaryotic phytoplankton as a function of ambient P_i concentrations.

Figure S6. *In situ* P_i uptake rates for the whole community. The samples are taken across the Western North Atlantic Ocean region ($n = 250$) at depths less than 50 m. The solid line represents a simple linear regression with an intercept = 0.

Figure S7. Biodiversity model evaluations. A. Pairwise invasibility plot (PIP) obtained with the evolutionary model that includes acclimation, with a *Synechococcus* parameterization and $w=0.5$; yellow regions indicate values of resident and invader sizes for which the resident is outcompeted, whereas the resident resists invasion in the black regions. B. Evolutionarily stable strategy (ESS) obtained with the eco-evolutionary framework with a *Synechococcus* parameterization and $w=0.5$; for all the different replicates of the numerical simulation, the reached ESS coincides with that obtained with the pairwise invasibility plot.

Table S1: Whole community and population-specific phosphate uptake kinetics and cell quota values from samples in the Western North Atlantic Ocean.

Sample	Station	Latitude	Depth (m)	Date	P_i (nM)		V_{max}[1] (nM/h, amol/cell/h, pmol/cell/h)	K_s (nM)	R^2	α (V_{max}/K_s)	Q_p[2] (nM, amol/cell, pmol/colony)	V_{max}/Q_p (d^{-1})
1	BV46 20	39.7°N	5	10/2/11	0.5	Whole com.	2.1	6.3	0.92	0.33	8	6.6
						Prochlorococcus	10.2	12	0.98	0.83	28	8.7
						Synechococcus	52	21	0.96	2.45	239	5.3
						Eukaryotes	121	26	0.95	4.60	1743	1.7
2	BV46 BATS	31.7°N	5	10/6/11	0.5	Whole com.	2.1	3.8	0.94	0.53	10	5.2
						Prochlorococcus	11.9	3.2	0.92	3.72	29	9.8
						Synechococcus	70	15	0.92	4.55	220	7.7
						Eukaryotes	77	41	0.95	1.86	6474	0.3
3	BV46 12	21.7°N	5	10/13/11	0.5	Whole com.	1.2	7.4	0.94	0.16	13	2.2
						Prochlorococcus	9.4	2.8	0.94	3.37	8	27.9
						Synechococcus	33	7.4	0.93	4.49	111	7.2
						Eukaryotes	475	185	0.91	2.57	4198	2.7
						Trichodesmium	30	96	0.95	0.31	3	0.2
4	AE1206 Eddy	32.8°N	5	3/17/12	0.9	Whole com.	1.5	16	0.93	0.10	16	2.3
						Prochlorococcus	1.3	3.4	0.93	0.38	-	-
						Synechococcus	5.6	2.5	0.93	2.29	-	-
						Eukaryotes	15.6	114	0.96	0.14	-	-
5	AE1206 BATS	31.7°N	5	3/19/12	0.7	Whole com.	1.3	2.1	0.97	0.64	12	2.6
						Prochlorococcus	2.5	0.8	0.87	2.92	-	-
						Synechococcus	27	5.1	0.96	5.24	-	-
						Eukaryotes	70	177	0.96	0.40	-	-
6	AE1206 BATS	31.7°N	80	3/19/12	8	Whole com.	0.13	26	0.97	0.005	15	0.2
						Prochlorococcus	1.2	32	0.97	0.04	-	-
						Synechococcus	1.2	24	0.95	0.05	-	-
						Eukaryotes	6.7	21	0.95	0.32	-	-
7	AE1319	55.0°N	5	8/25/13	150	Whole com.	1.2	26.6	0.88	0.05	90	0.3
						Prochlorococcus	-	-	-	-	-	-
						Synechococcus	44	32.3	0.96	1.36	-	-
						Eukaryotes	76	51.5	0.98	1.47	-	-
8	AE1319	45.0°N	5	8/28/13	50	Whole com.	1.2	30.4	0.96	0.04	37	0.8
						Prochlorococcus	-	-	-	-	-	-
						Synechococcus	38	38.4	0.99	0.99	-	-
						Eukaryotes	87	81	0.98	1.07	-	-
9	AE1319	39.0°N	5	9/03/13	0.5	Whole com.	1.2	8.1	0.87	0.15	10	3.0
						Prochlorococcus	16	3.5	0.99	4.54	-	-
						Synechococcus	37	19	0.88	1.92	-	-
						Eukaryotes	9.6	17	0.97	0.55	-	-
10	AE1319 BATS	31.7°N	5	9/08/13	0.5	Whole com.	2	4.5	0.98	0.44	10	4.9
						Prochlorococcus	16	4.4	0.98	3.66	-	-
						Synechococcus	119	9.9	0.96	12.00	-	-

							Eukaryotes	100	18	0.97	5.60	-	-
11	BV46 6	27.7°N	<25m	10/9/11	0.5	*Trichodesmium*	28	639	0.98	0.04	2.3	0.3	
12	BV46 8	25.7°N	<25m	10/10/11	0.6	*Trichodesmium*	55	246	0.8	0.22	2.1	0.6	
13	BV46 10	23.7°N	<25m	10/11/11	0.4	*Trichodesmium*	17	142	0.92	0.12	1.6	0.3	
							Whole com.	1.5±0.6	12±10		0.3±0.2		
							Prochlorococcus	8.4±6.4	3.8±3.8		2.4±1.7		
			Average values				*Synechococcus*	47±34	17±13		3.9±3.4		
							Eukaryotes	115±137	79±67		2.0±1.9		
							Trichodesmium	33±16	342±247		0.1±0.1		

[1]The unit for V_{max} is nM/h for the whole community, amol/cell/h for specific unicellular populations, and pmol/colony/h for *Trichodesmium*

[2]The unit for Q_p is nM for the whole community, amol/cell for specific unicellular populations, and pmol/colony for *Trichodesmium*

Table S2. Taxon-specific and group-specific allometries used in the eco-evolutionary model and compilation of observed and model-emergent biovolume and maximum growth rates for the different taxa considered in this work.

	Model parameters				Observed and emergent behavior			
	a_K (nM)	b_K	a_μ (d^{-1})	b_μ	Observed size (μm^3)	Observed μ_{max} (d^{-1})	Emergent size range for P_i<20nM (μm^3)	Emergent μ_{max} (d^{-1})
Prochlorococcus	3.98	0.30	0.75	-0.3	0.07	0.70	0.001-0.15	0.51
Synechococcus	3.98	0.30	3.00	-0.3	0.50	1.00	0.001-3.5	0.72
Picoeukaryotes	2.00	0.56	1.50	-0.2	8	0.6-1.2	0.001-22	0.58
Nanoeukaryotes	2.00	0.56	8.00	-0.2	180	0.6-1.8	0.001-280	1.35